Topological optimisation and 3D printing of a Bladed disc

Vincent Barreau, Enora Denimal, Loic Salles

V. Barreau, E. Denimal, L. Salles, Topological optimisation and 3D printing of a Bladed disc, Proceedings of the ASME TurboExpo 2022.

Topological optimisation and 3D printing of a Bladed disc

Vincent Barreau[1], Enora Denimal[2,*], and Loic Salles[1]

[1] *D*ynamics Group, Department of Mechanical Engineering, Imperial College London, London, United Kingdom
[2] *C*OSYS-SII, I4S,Univ. Gustave Eiffel, Inria, Campus Beaulieu, 35042 Rennes, France
[*] *C*orresponding author: enora.denimal@inria.fr

Abstract

In turbomachinery, components are pushed to their limits to meet more stringent specifications in order to increase their performances. In this context, structural topology optimisation is a promising technology as it improves substantially the mechanical properties while drastically reducing the mass. With the coming of additive manufacturing, optimised geometry can be manufactured making this technology even more attractive. The aim of this work is to investigate the potential of topology optimisation to optimise a full bladed disc to improve its dynamic performances in terms of mass, stress and modal coincidences.

The topology of a 3D-Finite Element Model of an academic bladed disc is optimised in this work and experimental validation is expected. So first, the disc is designed to fit in the test-rig and the mechanical integrity of the 3D-printed disc is experimentally verified. Second, the topology of the blades is optimised. Based on a trial-and-error process, the appropriate topology optimisation problem properties for vibration optimisation are identified. Thus, adding a static force at the blade tip forces a better material distribution over the domain and increases the blade stiffness. To minimise the number of coincidences, a numerical strategy based on iterative topology optimisation simulations is proposed to identify the correct set of frequential constraints. Final results show that the mass of the blade is reduced up to 32% and the number of frequential coincidences is reduced from 11 to 4. Final geometries are 3D-printed and mounted on the disc.

1 Introduction

The aeronautical industry is undergoing major transformations, particularly to reduce its environmental impact. In this context, a lot of efforts are dedicated to the optimisation of aircraft engines components. *Parameter optimisation* [1, 2] can be carried out on existing structure on a few key parameters. Only a light modification of the design is expected and a few percent improvement of the performances are expected. With *shape optimisation*, the general layout of a component can be optimised for a pre-defined connectivity [1, 3]. It is admitted that with shape optimization, the gain in performance is between 10% and 40% for common design problems [4]. More recently, the concept of *topology optimisation* has emerged and allows for deep modification of the nature of the structure as the geometry of the structure is not initially predefined as well as its connectivity [1, 5]. With this, it is expected to get an improvement in performance of 40% up to 100% [4]. Topology optimisation usually produces structures with exotic shapes with many holes. With the coming of additive manufacturing, it is finally possible to manufacture these optimal components. In this context, both have gained a lot of interest over the last years.

In aircraft engines, one key structure is the bladed disc. It is subjected to numerous extreme loads (vibration, thermal, stress, etc.) and the design of the latter is complex. The modal density of such components is high and all resonances cannot be avoided. It implies the control of the level of vibration et resonance with dedicated technologies such as friction dampers [5, 6]. This work demonstrates the potential that topology optimisation can offer to the aircraft industry for the design of bladed discs considering structural and vibratory constraints. In this context, the first work that has considered the use of topology optimisation for blades is [7]. In the latter, the blade geometry was simplified to a thick plate clamped at its base. Topology optimisation was conducted in 2D to optimise the first natural frequency and the maximum stress from a bird strike. Even though the geometry was simplified, results were promising. Then in [8], topology optimisation was considered for a full bladed disc for a static loading and a dynamic loading, both obtained from CFD simulations. However, no work has been dedicated to the optimisation of a full bladed disc with regard to (w.r.t.) vibration design

Figure 1: Rotating test-rig

considerations to minimise the number of critical speeds. More specifically, this work has for objective to explore the potential that offers topology optimisation for an entire bladed disc structure to mitigate stresses due to system resonances in rotating conditions.

Topology optimisation consists in the determination of the optimal material distribution in a given design domain for given boundary conditions and loads [1]. Different strategies exist to perform topology optimisation. The first family of methods is often called density-based methods [9]. They rely on the optimization of the densities of the elements of a mesh w.r.t. an objective functions and constraints. These methods are the ones implemented in industrial software. The second family of methods are based on the propagation of a level-set function by solving iteratively the Hamilton-Jacobi equation [10]. The iterations are based on the shape sensitivity of the level-set function w.r.t. the objective functions and constraints. More recent methods are based on evolutionary algorithms [5, 6, 11, 12]. One main objective of this work is to see if current capabilities of current commercial software are enough to optimise the topology of a full bladed disc considering system resonances in rotating condition. So the most popular topology optimisation method is adopted, namely the Solid Isotropic Material with Penalization (SIMP) method [9]. The OptiStruct Altair software is employed in this work to ensure an efficient and reliable implementation of such optimisation algorithm. Details about the theory of the SIMP method are given later on.

The objective of this work is to explore the potential of structural topology optimization in turbo-machinery, and more specifically for full bladed disc structures, to improve their dynamic performances in terms of mass, stress and modal coincidences, and to validate experimentally the numerical developments. Another objective, is also to develop a numerical process to realise such optimisation with current and existing tools for topology optimisation in the market. The objective is to see if current commercial software have the capability to answer such optimisation problem or if new developments are required. The experimental test-rig that will be used is represented in Fig. 1. An academic bladed disc is considered for the topology optimisation, and is represented in Fig. 2. In this work, the aerodynamic loadings are neglected to focus only on structural and vibrational considerations. This choice is also motivated by the fact that experiments will be carried out in vaccum. So, the airfoil skin of the blades is not considered in this work and it is assumed that the internal section of the blades is enough to optimise and to test the mechanical properties. One can see that the blades are located in grooves in the disc. In order to have a system that fits in the test-rig, a specific disc must be designed. The main constraints are related to the available space and the centrifugal loading. The parametric design of the disc and experimental validation will be done first and are detailed in Section 2. After that, the topology optimisation of the blades is performed. Two studies are conducted first for static analysis to optimise the blades w.r.t. to centrifugal loading and bird strike, to illustrate the interest of topology optimisation. Then, the topology of the blades is optimised to meet a frequency constraint to mitigate resonances. A trial-and-error process is adopted to identify the correct objective function, constraint functions, static loading and dynamic loading that must be considered to obtain reliable results. The full process is detailed in Section 3. Finally, the optimal disc and two optimal blade geometries are 3D-printed.

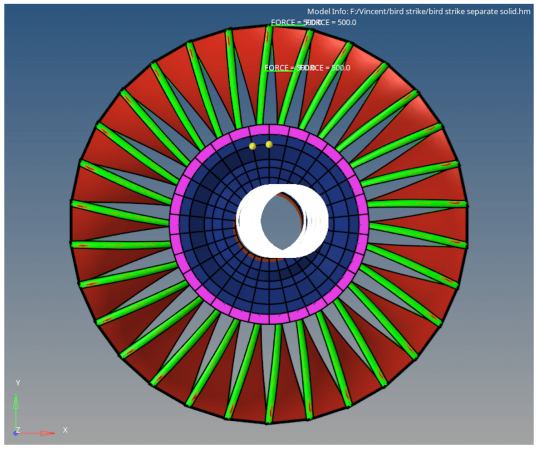

Figure 2: CAD of the non-optimised bladed disc

2 Design of the disc

This section is dedicated to the design of the disc to ensure the bladed disc can be mounted and tested on the existing rotating test-rig.

2.1 Numerical design of the disc

The section of the disc is based on a simplified version of [13]. The parametrisation of the shape is given in Fig. 3 and parameter description are given in Table 1. It was chosen to keep angles of 45 or 90 degrees between consecutive faces to reduce the number of parameters in the design. By using these parameters, the study is close to the traditional design of turbine discs, which ensures a realistic design. As the disc must fit in the existing test-rig and more specifically on the telemetry holder, some section parameters are imposed. Hence, the value of H_1, i.e. the inner radius, is imposed. The thickness T_3 on the upper part is imposed by the maximum depth allowed in the test-rig and by the depth of the blades, and is equal to 40 mm. Additionally, the number, the location and the size of screws used to fix the disc on the telemetry holder are known and so H_2 is taken to ensure a sufficient contact surface for the nuts and is equal to 20 mm. Also, to limit the risks of disc burst, which takes place at the outer diameter, the height of the top of the disc H_3 was also constrained at 20 mm to ensure the mechanical strength of this zone, which is the zone with the blade/disc junctions. T_1 was also imposed and fixed as equal to the thickness of the telemetry holder base. Finally, with the different constraints coming from the test-rig, the number of parameters to determine is equal to 2, namely T_2 and H_4. The CAD geometry of the disc and telemetry holder before the design is given in Fig. 4(a), where only the green part can evolve.

A parametric scan over the parameters T_2 and H_4 is performed and the configuration that ensures a maximum

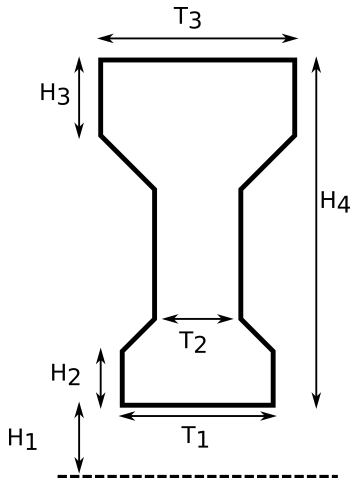

Figure 3: Disc section parametrisation [13]

Name	Description
T_1	Thickness of the bottom part
T_2	Thickness of the central junction
T_3	Thickness of the upper part
H_1	Inner radius
H_2	Height of the bottom part
H_3	Height of the top part
H_4	Total height of the disc

Table 1: Parameters of the disc section

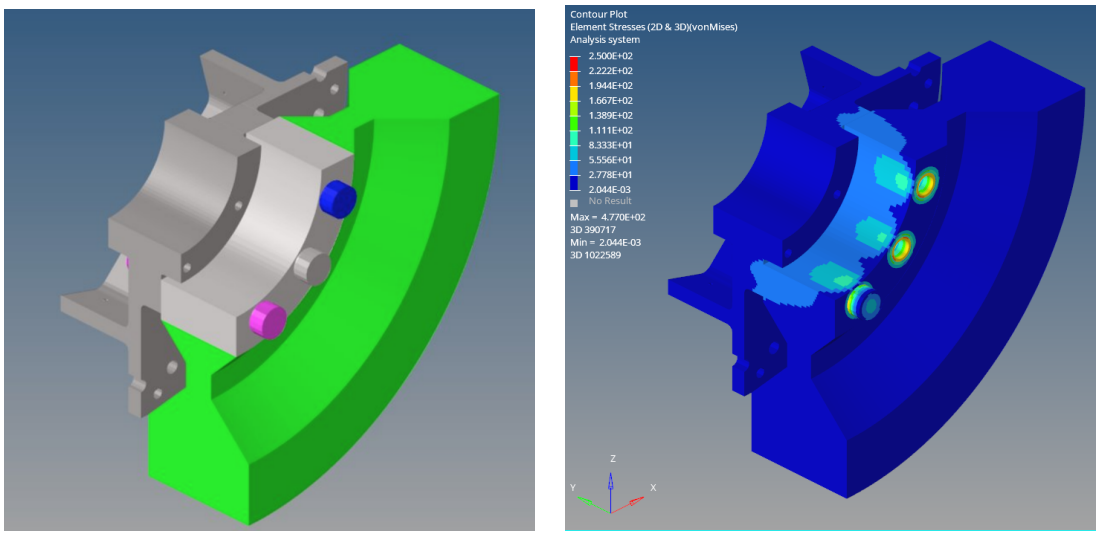

(a) (b)

Figure 4: CAD geometry of the assembly before (a) and after (b) the shape optimisation

stress inferior to $(\frac{1}{2}\sigma_Y)$ is taken, where σ_Y is the von Mises yield stress limit. To get all the mechanical constraints in the disc, the telemetry holder, the screws and nuts are present in the modelling. However, to ensure reasonable computational times, the blades are absent at this stage and the radial force exerted by the blades caused by the rotation was simulated by applying pressure on the outer surface of the disc. In terms of material, steel is chosen for the disc and the blades. Because 3D printing is carried out using plastic in the current work, it was chosen to use steel in the simulation for the disc and the blades to get a design valid for future studies with steel components. In terms of loading, contact and pretension in the bolts were introduced. Finally, only the geometry in green in Fig. 4(a) evolves. The section after optimisation is given in Fig. 4(b).

As the disc geometry was simplified and blades were absent, the optimal disc geometry still must be validated with the blades and the real connections to the disc. The study of the design of the disc/blade link is very complex and not essential for the realization of this project. However, it is still required to guarantee the mechanical integrity of the disc and the blades with the joints. Thus, it was chosen for all designed geometries to rely on pre-existing geometries. Two geometries have been retained: the dovetail and the firetree. They are shown in Fig. 5. It was chosen to have the two types of contact geometries on the disc for later experiments and future potential comparison of the contact shape. For this reason, it is chosen that dovetail and firetree links alternate on the disc, and the final distribution can be seen in Fig. 7. In order to ensure the mechanical strength of the assembly, studies in several different configurations were carried out. Only interesting and critical cases have been tested, and only two of them are presented here. Simulations are done with a rotational speed of 42 Hz. This speed is chosen based on the maximum rotational speed of the test-rig and to avoid the 50 Hz. The validation is made by checking that the stress levels in the disc and blades are acceptable for steel and resin material.

To simplify the analysis, it was considered that the stress induced by the telemetry holder/bladed disc junction would not have any influence on the part of the disc studied here, so this junction was replaced by a constraint on the inner part of the disc. This assumption has been tested and verified by doing the simulations with and without the telemetry holder modelling.

Two test cases, representative of future critical experiments, are presented here. The first one corresponds to the worst case scenario in terms of stress levels in the disc. It is reached when the blades are located on adjacent grooves with different link geometries. The presence of a hole to fix a ring that prevents the blades from sliding out during the test implies higher stress levels. The stress distribution is this area of the disc is displayed in Fig. 6(a), with a maximum equal to 51 MPa, well below the tensile stress of the steel. The second test case corresponds to a future experimental setup where only one type of junction is present, i.e. five blades are distributed around the disc and some junctions are empty. Stress levels for the case of the dovetail are presented in Fig. 6(b). Despite the increase in stress, the stress levels remain acceptable and so even with a low number of blades, the mechanical strength of the disc is ensured. In all cases the maximum stress levels remain largely inferior to the tensile stress of the steel, which validate the chosen design. Similar results are obtained with the blades made of resin and the disc made of polyamide to ensure that the printed components also verify

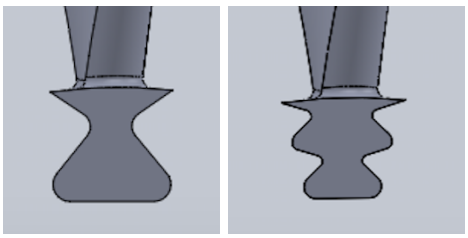

Figure 5: Final geometry of the dovetail (right) and firetree (left)

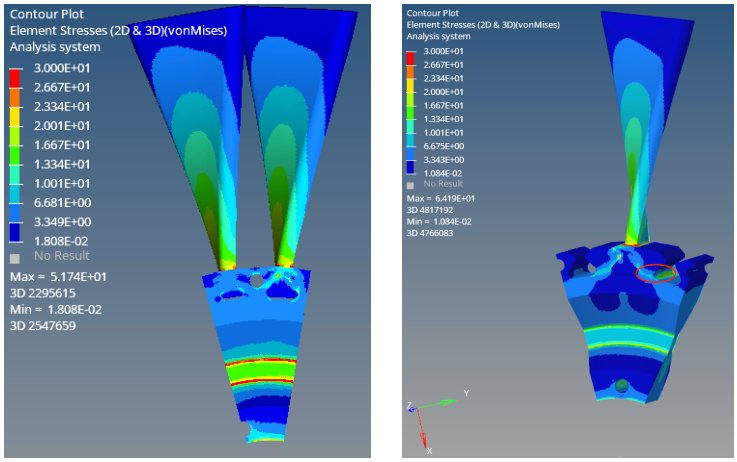

(a) (b)

Figure 6: Stress induced by the rotation of the blades for the first (a) and second (b) scenario - (a) Dovetail geometry on the right and firetree on the left - (b) dovetail geometry

the mechanical strength.

2.2 Experimental tests

In a second stage, the mechanical properties of the disc were experimentally verified. The disc was 3D-printed in polyamide by a private company and it is visible in Fig. 7. To ensure the integrity of the disc during the experimental tests, the blades are made of a resin with lower performances than the disc material. To validate experimentally the mechanical integrity of the disc, these tests were necessary because the properties of the material used for the disc are not available. The particular geometry of the bond also makes the test more difficult than the theoretical approximation or Finite Element Analysis (FEA). All blades and mechanical components other than the disc were printed using a 3D-printer available in the laboratory. It uses the principle of Stereolithography i.e. an ultraviolet laser reacts a photopolymer layer by layer. This printer has an accuracy of 25 μm.

During the 3D-printing of the blades, a specific attention has been put on the location of the support required for printing as they leave marks (low surface finishing and so no flat surface) even when removed and so alter the quality of the final print. This is particularly important in contact surface areas. After printing, blades are put in an alcohol bath to be cleaned. It is then possible to do a treatment, similar to an annealing, so that the parts reach their maximum mechanical strength properties.

To test the disc and blades behaviour, a dummy geometry of the blades was printed, it is displayed in Fig. 8a. Only a section of the disc with a blade was tested, and this was replicated for each junction geometry (dovetail and firetree). The mechanical strength of the disc sections was tested with tension tests, where loading is applied directly on the dummy blades as it can be seen in Fig. 8a. A general view of the setup can be seen in Fig. 8b. The disc is held in place by a press (see Fig. 8a) and the loading is applied by a weight placed on the shackle (see Fig. 8b). The general objective is to ensure that blades fail first. To do so, a load equivalent to the maximum centrifugal loading is applied to the dummy blade. It was approximated from the numerical simulations, that the force exerted by the centrifugal force during the rotation of a blade at 42 Hz is approximately 300 N. To ensure the mechanical strength of the printed material, it was chosen to select a material that could withstand at least twice this load. The blade was loaded up to 1400 N (to test it and also to see where the fracture would

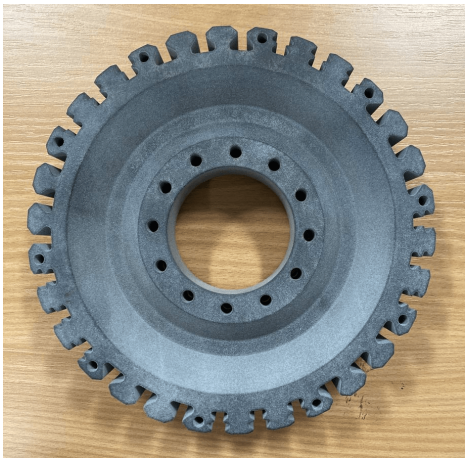

Figure 7: Printed disc

(a) (b)

Figure 8: Experimental testing of the disc and blade resistance under tension - (a) zoom on the disc and blade section - (b) full assembly

occur) for the two link geometries. In neither case did one of the two pieces break, which proves on the one hand that the strength of the disc is sufficient and on the other hand that the strength of the blade and the blade/disc junction is sufficient. During operating conditions, fretting fatigue is expected but it is neglected here, and dry lubricant would be used for the experiments to limit it.

3 Topology optimisation of the bladed disc

As the disc has been designed, the topology of the blades can be optimised. The topology optimisation was performed with the software Optistruct using the SIMP method, briefly described in the following. Depending on the objective function and the constraints, the density of each element of the design domain are updated until the optimal topology is reached. Different cases for topology optimisation have been investigated here. A first case study was done as a validation test case, and compared to literature results. It corresponds to the minimisation of the compliance when the blades are rotating. The second case corresponds to the case of bird strike. Finally, a trial-and-error strategy is developed for the topology optimisation of blades for dynamic analysis to avoid any resonance of the blades. It is reminded here that the aerodynamic effects are neglected and so the airfoil skin is not considered in this work. The objective is to focus only on the structural part and so it is assumed that the internal section of the blade is enough to optimise and test the mechanical properties.

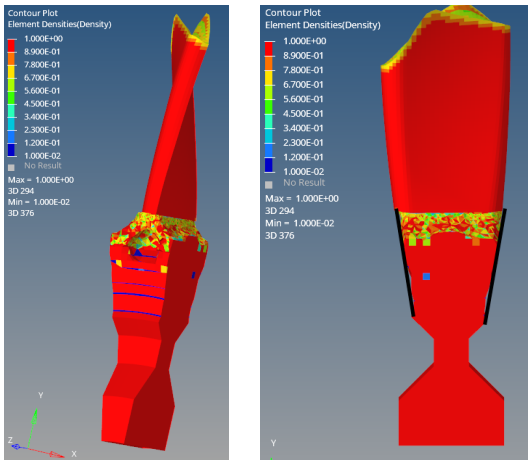

(a) Front of the blade (b) Side of the blade

Figure 9: Case 1 - Optimised geometry of the disc and blades - (a) Front view and (b) side view

3.1 Topology optimisation with the SIMP method

The topology optimisation method adopted in this work is the popular SIMP method, implemented in almost each commercial software. A brief description of the method is given here for the sake of concision, for more details refer to [14].

Density-based topology optimisation methods rely on a FEM of the design domain. The optimisation variables are the material densities of each mesh element. Ideally, the variables are binary, but it causes strong difficulties in the resolution of such optimisation problem. One solution is to model these densities as continuous variables that take value between 0 (void) and 1 (full material), and gradient based optimisation methods able to deal with a large number of variables are applied. With the SIMP approach, the material properties are also modelled as continuous variable with an interpolation with a power law. For example, the Young's modulus E_i of an element i is given by: $E_i = E_0 + \rho_i^p(E_1 - E_0)$. The interpolation parameter p is taken between $[1, 3]$, ρ_i is the material density of the element i, E_1 is the Young's modulus of the material $E_0 \ll E_1$ is the Young's modulus of the void domain (not equal to 0 for gradient computation).

3.2 Topology optimisation for static analysis

3.2.1 Centrifugal loading

The first case consists in the minimisation of the compliance when the disc and the blades are rotating at 42 Hz. As it is a static analysis, a fine mesh can be used with more than 1,450,000 elements to get an accurate description of the final geometry. The disc and the blades are in the design domain. Optimisation is carried out with the following properties: the volume fraction is constrained between 0.5 and 0.8, and a maximum stress constraint of $\sigma_Y/2$ is applied and the SIMP interpolation parameter p is taken equal to 3 here.

Results obtained after optimisation are given in Fig. 9. Elements with a density inferior to 1E-2 are not displayed. Elements full of material are in red, and intermediary densities are in yellow and orange. One can see that material is removed from the top of the blades, which is expected here. Indeed, the further away from the axis of rotation, the greater the centrifugal force and therefore the greater the displacement and therefore the higher the compliance. So a reduction of the density far from the axis of rotation decreases the compliance. Similar results are obtained in [8], which gives confidence in the results here. Moreover, one can see that at the bottom of the blades, intermediary densities are present. More particularly, one can see a hole between the blade and the disc on the front view (see Fig. 9. A similar hole is visible on the other side, but is smaller. This is easily explained by the nonuniform mass distribution of the blade.

3.2.2 Bird Strike

In a second case, a topology optimisation of the blade for a bird strike loading case is performed. The bird strike is modelled by a static pressure on the blades [7].

To ensure the well-posedness of the mechanical problem, the external surface on the blade edges is removed from the design domain to ensure the presence of the surface on which the pressure is applied. The disc is also

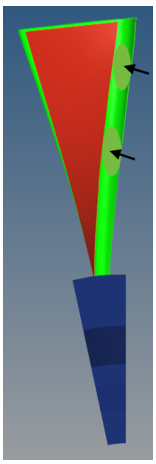

Figure 10: Design domain of the blade for the topological optimisation of the bird strike - disc (blue), design domain (red) and fixed domain (green)

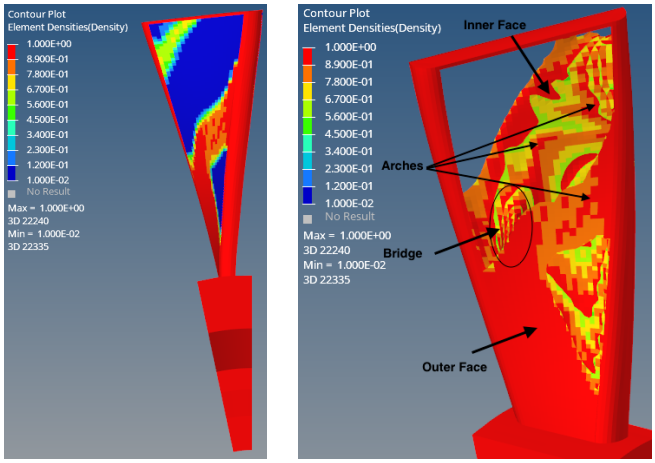

(a) (b)

Figure 11: TO for bird strike - Density distribution on the outer surface of the blade (a) and in the interior of the blade (b)

removed from the problem here. The design domain is represented in Fig. 10. The design domain is in red, the disc in blue and the external surface removed from the optimisation in green. A pressure of 1 kN in applied on the black green part indicated by arrows. The modelling choice is based on [7]. The optimisation consists in the minimization of the compliance, and the following constraints are applied: the mass fraction is imposed between 0.1 and 0.5, a minimum thickness of 1 mm for the final geometry is imposed and a maximum stress constraint of $\sigma_Y/2$ is also imposed.

Results are displayed in Fig. 11 where the material density of the outer surface is given in Fig. 11(a) and a view on the material distribution inside the blade is given in Fig. 11(b) (densities inferior to 0.5 are not displayed). Looking at Fig. 11(a), one can see that a lot of material is removed and two arms remain in the structure. This can be considered as quite similar to results obtained in [7] from a 2D topology optimisation. However, when looking at the interior of the blade, the structure is more complex. Indeed, the internal domain is not empty and sort of arches are present (indicated by arrows). They are not present in the results from [7], which demonstrates the importance of considering the real 3D geometry for such optimisation. Moreover, one can see that different bridges seem to connect the different arches. Results are consistent as with the load case, the stress levels experienced by the inner face are higher than for the outer face, and so more material is expected to respect the stress constraint. To increase the stiffness of the blade and to counterbalance the stresses applied to the blade, the red part of the outer face is completely filled.

Rotational Speed [Hz]	Frequency [Hz]	ND
42	2130	8
	2410	9
	3150	12
	3660	14
20	127	1
	240	2
	3470	1
	3800	2
10	126	1
	1917	2
	3700	3

Table 2: Excited Frequencies with full blades

3.3 Topology optimisation for dynamic analysis

In this section, topology optimisation is set up for dynamic analysis. First, the determination of the appropriate constraints and loadings to get reliable results is done based on a trial-and-error methodology. In a second time, an advanced frequency constraint strategy is developed for the final topology optimisation of the blade. Finally, two optimised geometries of the blades are 3D-printed and assembled in the 3D-printed disc.

3.3.1 Determination of the topology optimization properties for dynamic analysis

First, a Campbell diagram and a Singh's Advanced Frequency Evaluation (SAFE) diagram are computed to determine the natural frequencies of the bladed disc that could be excited. This is done for different rotational speeds and results are summarized in Table 2. The aim of this study is to keep the natural frequencies of the optimised blades as far away as possible from the natural frequencies of the excited blades. It is important to note that the frequencies under 3500 Hz are optimised as it would not have been possible to detect higher frequencies in the tests.

For dynamic analysis, compliance cannot be used as an objective function anymore and the minimisation of the volume must be used as the objective function, which sometimes results in geometries with very low mechanical properties, as low stiffness or low mechanical strength. Therefore, other constraints must be used, with the risk of over-constraining the optimisation and not being able to carry it out. In a first time, a constraint on the Frequency Response Function (FRF) has been considered, but it requires a too high computational time. So the strategy adopted relies on a frequency bound constraint for each mode as it implies only the computation of the natural frequencies. This constraint means that the frequency f_i of a mode i must remain in the interval $[f_{min}^{(i)}, f_{max}^{(i)}]$. These intervals are based on the natural frequencies of the non-optimised case and intervals are chosen so that the frequencies are not in possible frequency excitation ranges. Additional constraints, on stress, displacements, etc., must also be added. To determine the good combination of the latter, different cases have been considered and are all summarized in Table 3. For all these cases, the different frequency bounds for the different modes are kept constant.

The following results have been obtained for the different cases and representative results are displayed in Fig. 12. For Case 1, it appears that the constraints on the frequency were not verified. Moreover, the material distribution in the blade is not satisfactory as the upper part of the blade is empty (see Fig. 12(a)). To compensate this, in Case 2, a minimum mass fraction of 0.5 is impose to ensure the presence of more material. Results are slightly improved but the upper part of the blade is still empty as for Case 1, and so this choice is not satisfactory. In Case 3, it was chosen to constrain the dimension of the material domain between 1 and 3 mm to avoid large parts of material in the bottom of the blade and to remove the top surface of the blade from the design domain to force the presence of material in this area. However, it creates large areas with intermediary densities and so the shape of the blade is not easily interpretable. For Case 4, a strategy based on the modification of the design space was considered. The top surface of the blade is removed from the design domain, and the rest of the blade is divided into two design domains, one in the upper part and another in the lower part. Each part has the same constraint, which impose on having a significant density in the upper zone. However, it tends to create separate sections and there is still a void in the upper part of the blade and so the strategy is not retained. In the Case 5, the radial draw constraint was tested as it indicates a preferred direction (here radial), however results were unsatisfactory with large areas of intermediary densities and a lack

Case Number	Specifications	Case Number	Specifications
1	minimum dimension 5 mm stress <24 MPa	6	minimum dimension 5 mm stress <24 MPa mass fraction >0.7 blade tip radial displacement constrained
2	minimum dimension 5 mm stress <24 MPa mass fraction >0.5	7	setup 3 penalisation parameter between 3 and 4
3	dimension between 1 and 3 mm stress <24 MPa mass fraction >0.5 top of the blade not in the design domain	8	minimum dimension 5 mm stress <24 MPa blade tip radial displacement constrained frequency constraints up to 4000 Hz (instead of 3500 H
4	stress <24 MPa mass fraction >0.5 top of the blade out of the design domain design domain separated in 2	9	setup 8 tangential displacement constraint (due to a new tangential pressure at the blade tip)
5	minimum dimension 5 mm stress <24 MPa radial draw constraints		

Table 3: Summary of the different properties for the different topology optimisation setups

of material in the upper part of the blade. As the modification of the constraints or of the design domain proved to be inefficient, it was considered to add a displacement constraint on the blade tip with a higher mass fraction for the Case 6. This is done by adding a static load at the tip blade. By adding this new load, it is expected to increase the stiffness of the final geometry. The load is chosen arbitrarily and is normal to the top surface. The maximum displacement constraint is set to $0.5d_{full}$, where d_{full} is the blade tip displacement of the full blade with the chosen load. Results are displayed in Fig. 12(b). While the results are not perfect as large areas of intermediary densities are visible, they were promising as the material distribution is shifted in the upper part of the blade. The addition of a displacement constraint from a static load forces the increase of the blade stiffness with a material distribution over the full blade, opposite to previous cases where material was only in the lower part of the blade. In the Case 7, the strategy was kept and the penalisation parameter of the SIMP law was changed, but it did not give interesting results (large areas with intermediary densities). So the Case 6 is used as a starting point of the Case 8 but the frequencies are constrained up to 4 kHz, instead of 3.5 kHz, and the mass fraction constraint is removed. Results are displayed in Fig. 12(c) and are very satisfying as material is distributed on the full blade and empty areas are clearly distinguishable. The stress distribution in the blade is also satisfactory and results are obtained without a mass fraction constraint. A last case was considered, were a tangential displacement constraint is also added which comes from a tangential pressure applied on the top of the blade. The purpose of this constraint is to increase the stiffness of the blade. Results are given in Fig. 12(d) and are even more interesting as it is close to the result of the Case 8 with simply smaller holes and therefore a fuller blade which makes the blade stiffer. This proves that by carefully positioning the areas where material will be removed, it is possible to preserve stiffness characteristics simply by varying the size of the holes while optimising the various properties of the blade.

3.3.2 Final strategy and results

Previous studies aimed at determining the set of constraints and objective function to choose to get consistent results for the topological optimisation of a blade for a dynamic analysis. As they have been determined, one must now focus on the frequency constraints.

In the previous studies, a constraint was imposed on each frequency and the latter had to be in a predefined interval. However, the modes are identified by an integer and during the optimisation, a switch between the different modes may happen and so the optimisation fails as the constraint is not applied on the targeted mode anymore. So the constraint is now applied on frequency gaps to avoid coincidence and an iterative process is adopted to determine the appropriate frequency constraints. Frequency constraints are applied on the gap between the modes to avoid coincidences. The iterative numerical strategy developed is presented here. A first topology optimisation is performed with a set of constraints. If from the results, the mode i appears to be

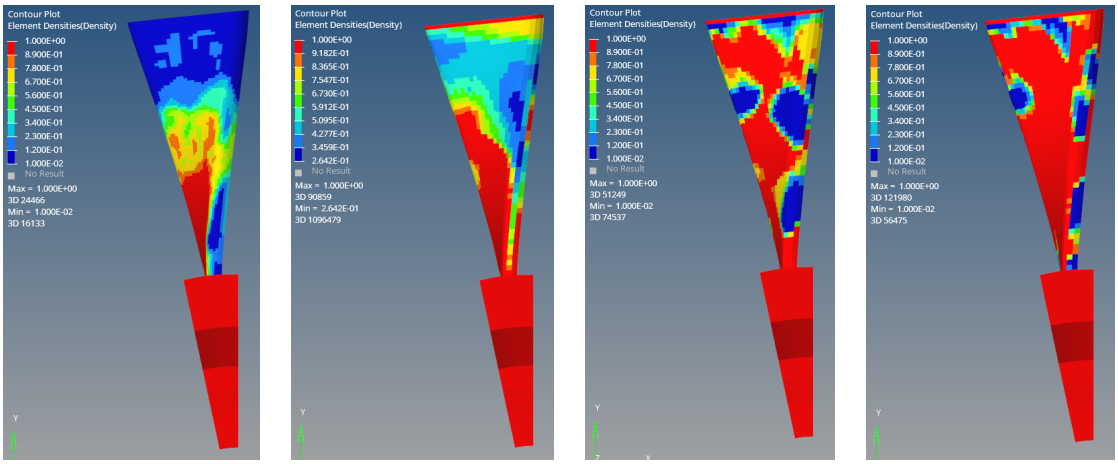

(a) Case 1 (b) Case 6 (c) Case 8 (d) Case 9

Figure 12: Density distribution for different topology optimisation setups - Displacement and mass constraint (a) - Displacement constraint only (b) - Application of force and displacement constraint (c)

in a forbidden frequency range $[f^k_{min}, f^k_{max}]$ and the mode $i+1$ is above, then a new topology optimisation is launched with the constraints $f_i < f^k_{min}$ and $f_{i+1} > f^k_{max}$ on the frequencies. In some cases, this formulation works and the constraint is kept. However, in some cases frequencies of modes i and $i+1$ cannot be separated. In this case, the constraint is applied on the modes $i+1$ and $i+2$ with $f_{i+1} < f^k_{min}$ and $f_{i+2} > f^k_{max}$. This iterative process is done until the coincidences are avoided. At the end of each iteration, the modes that are in a forbidden frequency range are identified and targeted in the next iteration. With this strategy, the problem of switching modes is avoided, but it constrains a lot the optimisation and requires numerous iterations. Indeed, at each iteration, a topology optimisation based on the setup 8 of Table 3 and with frequency constraints is performed.

The different results of the optimisation carried out are summarized in Table 4, where the number of coincidences between the natural frequencies and the excited frequencies are given at different optimisation steps. For indication, the number of coincidences for the non-optimised geometry and for the geometry of the setup 8 of Table 3 are also given. One can see that from an iteration to another, the number of coincidences tends to decrease. However, the coincidences do not necessarily occur for the same mode or Engine Order (EO). The different geometries of these iterations are shown in Fig. 13. One can see the evolution of the material distribution over the domain between the different iterations. At the first iteration, the upper part of the blade is almost empty, whereas at iterations 4 and 5, it is more spread. Results are quite different from those obtained for the setup 8 of Table 3 (see Fig. 12(c)), this illustrates the high impact of the constraint selection of the results. For a non-optimised blade, the number of coincidences is equal to 11, with the Case 8, eight coincidences are still present. Even though it corresponds to an important reduction of the number of coincidences, it is still consequent. With this strategy, only four coincidences are present at the end, which illustrates the interest of the approach. The global objective over the different iterations was to minimise the total number of coincidences as a design criterion, but another criterion could be preferred.

The new Campbell diagram is not shown here for the sake of concision, but all coincidences are avoided

Gap: Excited/Natural Frequency	**<1%**	**<2%**	**<3%**
Non optimised - Full blade	3	2	6
Setup 8	1	1	6
Iteration 1	3	2	5
Iteration 2	2	3	4
Iteration 3	3	2	4
Iteration 4	0	3	1
Final Iteration	1	1	2

Table 4: Number of excited frequencies for the different geometries derived from the topological optimisation

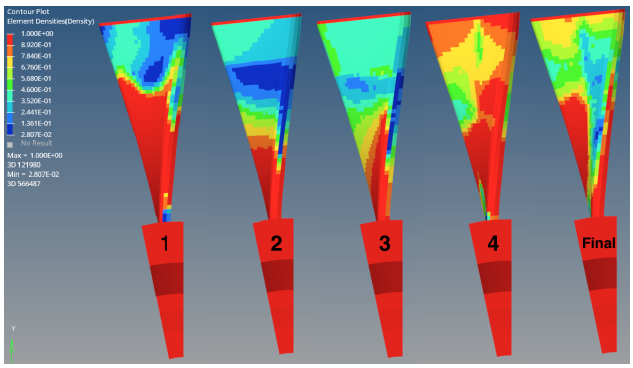

Figure 13: Geometry evolution of the optimisation result

compared to the non-optimised bladed disc. Indeed, more than 5% of frequency gaps are observable. This underlines very well the interest of topology optimisation. The possibility to reduce the number of excited modes, especially for high EO, and to reduce the mass of the blades by more than 10% demonstrates the interest of such an approach and highlights that topology optimisation could in the future, support the current trend of reducing the ecological impact of the aircraft industry.

3.3.3 3D printing of the blades

Two blade geometries were selected for printing. The first geometry corresponds to the results obtained with the Case 8, and the second geometry comes from the previous section with an advanced constraint on the frequencies. The blade geometries were extracted and recreated, and the CAD view of the two geometries in Solidworks are given on the left column of Fig. 14. It is clear that the geometries do not correspond exactly to the optimised ones. As the optimal geometry was complex, the shape was smoothed. The density limit was chosen equal to 0.75. It would have been useful to perform several tests to select the density limit that recreates exactly the simulation results, however this limit 0.75 was a good compromise in terms of mass reduction and efficiency. The blades are 3D-printed based on the methodology described in Section 2.2.

In terms of general comments, both geometries reduce drastically the number of frequency coincidences and thus potentially prevent any resonance of the blades. Additionally, they offer a significant weight saving. The weight is reduced by 15% for the results of Case 8 and by 32% for the advanced frequency constraint case. In addition to this, the centre of mass of these two blades is also 4 mm closer to the centre of rotation, which corresponds to a reduction of 10%. The reduction of this distance coupled with the mass reduction implies a considerable reduction in the stresses and forces induced in the blade by the centrifugal force. It means that less complex materials and heat treatments could be used as, for example, the stresses in the bonds would be lower. This reduction in stress also leads to a reduction in inertia and in the effort needed to rotate the bladed disc and to maintain this rotation. Therefore, less energy is needed for the different stages of the engine and therefore it is possible to have more thrust, or to use less fuel, which reduces the ecological impact of the aircraft. The displacement constraint, introduced at the beginning to fight against the lack of rigidity of the upper part of the blade, also allows the reduction of tip rubbing, which can also help to fight against one of the reasons of aeronautical losses.

Finally, the blades were integrated in the 3D-printed disc, the assembly is shown in Fig. 15 with the disc, the telemetry holder and 2 blades on the test bench.

4 Conclusion

In this work, the interest of topology optimisation for bladed disc w.r.t. vibratory design consideration was investigated. The optimal topology was intended to be tested on an existing rotating test-rig. In a first step, the disc was design in order to fit in the test-rig, but also to ensure the mechanical strength of the latter during the tests. Different configurations have been numerically tested, with more or less blades and with different blade/disc junctions. A final experimental validation was done on a 3D-printed disc section with a dummy 3D-printed blade. A resistance test under tension was performed to ensure the mechanical strength of the disc, the blade and the junction between the two components.

In a second step, topology optimisation of the blades was investigated. The aerodynamic effects are neglected and so the airfoil skin is not considered. First, two study cases were considered based on static simulations, namely for centrifugal loading and bird strike. Results from the centrifugal loading show that the optimal

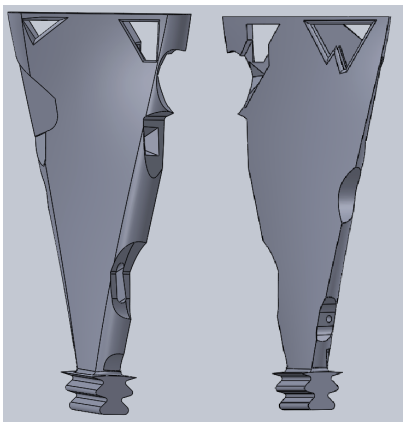

(a) Result of the Parametric Study-Solidworks

(b) Result of the Parametric Study - 3D printed

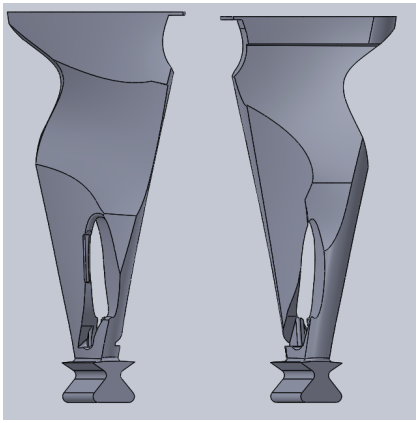

(c) Best Iteration of the Optimisation-Solidworks

(d) Best Iteration of the Optimisation - 3d printed

Figure 14: Optimised blades - CAD view (left) and 3D-printed geometries (right)

topology is based on a removal of the material in the upper part of the blade. Regarding bird strike, more complex topologies are obtained. Finally, topology optimisation w.r.t. to dynamic consideration is done. The appropriate set of objective function, constraints and loading to optimise the natural frequencies of the blades is identified based on a trial-and-error approach. It is demonstrated that considering a displacement constraint at the blade tip improves drastically the results obtained from topology optimisation. With this approach, the blade mass is reduced by 32% compared to the full blade. Moreover, the number of excited frequencies is reduced to 8, whereas it is equal to 11 for the non-optimised blade. To avoid any switch between the modes during the topology optimisation process, a constraint on the frequency gaps between the excitation frequency and natural frequencies is added. With this approach, the mass of a blade is reduced by 15% and the number of excited frequencies is reduced to 4. This mass distribution also leads to a reduction in the distance between the centre of mass and the axis of rotation, which reduces the centrifugal force and so the level of stress in the blade. The two optimal geometries are 3D-printed and mounted on the 3D-printed disc. Future works will be focused on the experimental validation of the numerical results.

This work demonstrates the potential of topology optimisation for the design of future aircraft engines components that satisfy complex and numerous technical specifications. In this work, breakthrough blades geometries that meet stringent specifications have been identified. The results are obtained on an academic bladed disc, but are promising for real-world applications. For future work, the aerodynamic effects should be considered.

Acknowledgments

E. Denimal and L. Salles thank Rolls-Royce plc and the EPSRC for the support under the Prosperity Partnership Grant “Cornerstone: Mechanical Engineering Science to Enable Aero Propulsion Futures,” Grant No.

Figure 15: Overview of the final assembly

EP/R004951/1. The authors would like to acknowledge Dr Luke Muscutt for his help with the experimental work and the 3D-printing.

References

[1] Niels Olhoff. On optimum design of structures and materials. *Meccanica*, 31(2):143–161, 1996.
[2] EP Petrov. Direct parametric analysis of resonance regimes for nonlinear vibrations of bladed disks. *Journal of Turbomachinery*, 129(2):495–502, 2007.
[3] W Song and AJ Keane. An efficient evolutionary optimisation framework applied to turbine blade firtree root local profiles. *Structural and Multidisciplinary Optimization*, 29(5):382–390, 2005.
[4] Pierre Duysinx. *Optimisation topologique: du milieu continu à la structure élastique*. PhD thesis, ULg-Université de Liège, 1996.
[5] Enora Denimal, Fadi El Haddad, Chian Wong, and Loic Salles. Topological optimization of under-platform dampers with moving morphable components and global optimization algorithm for nonlinear frequency response. *Journal of Engineering for Gas Turbines and Power*, 143(2):021021, 2021.
[6] Enora Denimal, Ludovic Renson, Chian Wong, and Loic Salles. Topology optimisation of friction under-platform dampers using moving morphable components and the efficient global optimization algorithm. *Structural and Multidisciplinary Optimization*, 65(2):1–19, 2022.
[7] J Meng, LF Liao, D Li, Y Cao, LY Yang, and YY Chen. Topology optimization method research on hollow wide-chord fan blade of a high-bypass turbofan engine. *Procedia Engineering*, 99:1228–1233, 2015.
[8] Enrico Boccini, Enrico Meli, Andrea Rindi, Lorenzo Pinelli, Lorenzo Peruzzi, and Andrea Arnone. Towards structural topology optimization of rotor blisks. In *Turbo Expo: Power for Land, Sea, and Air*, volume 51135, page V07AT30A008. American Society of Mechanical Engineers, 2018.
[9] Martin Philip Bendsøe and Noboru Kikuchi. Generating optimal topologies in structural design using a homogenization method. *Computer methods in applied mechanics and engineering*, 71(2):197–224, 1988.
[10] Michael Yu Wang, Xiaoming Wang, and Dongming Guo. A level set method for structural topology optimization. *Computer methods in applied mechanics and engineering*, 192(1-2):227–246, 2003.
[11] Yi Min Xie and Grant P Steven. Basic evolutionary structural optimization. In *Evolutionary structural optimization*, pages 12–29. Springer, 1997.
[12] Mariusz Bujny, Nikola Aulig, Markus Olhofer, and Fabian Duddeck. Identification of optimal topologies for crashworthiness with the evolutionary level set method. *International Journal of Crashworthiness*, 23(4):395–416, 2018.
[13] Dian-Yin Hu, Jun-Jie Yang, Cheng-Wei Fei, Rong-Qiao Wang, and Yat-Sze Choy. Reliability-based design optimization method of turbine disk with transformed deterministic constraints. *Journal of Aerospace Engineering*, 30(1):04016070, 2017.
[14] Martin Philip Bendsoe and Ole Sigmund. *Topology optimization: theory, methods, and applications*. Springer Science & Business Media, 2003.